Synthesis, Structural Characterization, Magnetic Behavior, and Single Crystal EPR Spectra of Three New One-Dimensional Manganese Azido Systems with FM, Alternating FM-AF, and AF Coupling

Morsy A. M. Abu-Youssef,[†] Albert Escuer,*[,‡] Dante Gatteschi,[§] Mohamed A. S. Goher,[||] Franz A. Mautner,[⊥] and Ramon Vicente[‡]

Chemistry Department, Faculty of Science, Alexandria University, Egypt, Departament de Química Inorgànica, Universitat de Barcelona, Diagonal 647, 08028 Barcelona, Spain, Dipartimento di Chimica, Universitá degli Studi di Firenze, Via Maragliano 75−77, 50144 Firenze, Italy, Chemistry Department, Faculty of Science, Kuwait University, P. O. Box 5969, Safat, 13060 Kuwait, and Institut für Physikalische und Theoretische Chemie, Technische Universität Graz, A-8010 Graz, Austria

Received June 7, 1999

Reaction of sodium azide with manganese(II) and pyridine derivatives such as 2-bzpy, 3-bzpy, and 3,5lut (2-benzoylpyridine, 3-benzoylpyridine, and 3,5-dimethylpyridine, respectively) led to the one-dimensional systems *cis*-$[Mn(2\text{-bzpy})(N_3)_2]_n$ (**1**), *trans*-$[Mn(3\text{-Bzpy})_2(N_3)_2]_n$ (**2**), and *cis*-$[Mn(3,5lut)_2(N_3)_2]_n$ (**3**). Compound **1** crystallizes in the $P2_1/n$ group: $a = 14.413(4)$ Å, $b = 16.157(4)$ Å, $c = 18.478(5)$ Å, and $Z = 12$. Compound **2** crystallizes in the $C2/c$ group: $a = 14.179(5)$ Å, $b = 9.698(4)$ Å, $c = 34.351(12)$ Å, and $Z = 8$. Compound **3** crystallizes in the $P2_1/n$ group: $a = 13.552(6)$ Å, $b = 7.730(3)$ Å, $c = 16.554(6)$ Å, and $Z = 4$. Structural determination shows a chain with double $\mu_{1,1}$ azido bridges for **1**, an alternating system with double $\mu_{1,1}$ and $\mu_{1,3}$ azido bridges for **2**, and finally a chain with double $\mu_{1,3}$ azido bridges for **3**. Susceptibility data show ferromagnetic coupling for **1**, antiferromagnetic coupling for **3**, and alternating ferro−antiferromagnetic interactions for **2**. EPR data measured on powdered samples and single crystals show the ideal Heisenberg narrowing angular dependence for the three kinds of coupled systems and an increasing dipolar broadening mechanism in the order **3** < **2** < **1** according to the decreasing Mn···Mn intrachain distances.

Introduction

Recent research on the manganese(II)−(L)−azido-bridged system, L = N-aromatic ligands, is providing an exceptional number of materials with new structural and magnetic features. When L is a pyridine ligand, infinite arrays characterized by different dimensionality can be obtained: 3-D for L = pyridine (py),[1,2] 2-D for L = 3- and 4-acetylpyridine (3-acpy[3] and 4-acpy[4]), methyl and ethyl isonicotinate (Meinc[5] and Etnic[2]), ethyl nicotinate (Enic[6]), or 4-cyanopyridine (4-CNpy[3]), and finally 1-D for 2-hydroxopyridine (pyOH), 3-ethylpyridine (3Etpy),[7] or 3-ethyl-4-methylpyridine (3Et-4Mepy).[8] Other 2-D or 3-D networks have been described with 4,4′-bipyridine[9] or bipyrimidine[10] ligands. The most common coordination mode of the azido bridge was found to be $\mu_{1,3}$-N_3 (end-to-end, EE), but it is not rare in these kinds of systems to find $\mu_{1,1}$-N_3 (end-on, EO) coordination mode simultaneously in the same compound, allowing alternated systems.[2−4,6,8,9] No correlation has so far been found between the properties of the L ligand and the coordination mode of the azido bridge. The magnetic behavior of these compounds follows the same general trends observed in either copper or nickel(II) systems; i.e., EE bridges lead to antiferromagnetic interaction,[7] and EO bridges give ferromagnetic coupling.[11] Systematic synthesis and magnetic study of pyridine derivatives have recently led to the characterization of low-temperature magnetically ordered phases with critical temperatures ranging between 16 and 40 K for several molecular-based magnets of general formula $[Mn(L)_2(N_3)_2]$ (L = py, 3- and 4-acpy, 3-Etnic, 4-CNpy).[2,3]

Following our research on compounds of this kind, we studied the derivatives obtained by reaction of the ligands L = 2- and 3-benzoylpyridine (2-bzpy and 3-bzpy) and 3,5-dimethylypyridine (3,5lut) with manganese(II) and sodium azide. From these reactions three new monodimensional systems *cis*-$[Mn(2\text{-bzpy})(N_3)_2]_n$ (**1**), *trans*-$[Mn(3\text{-bzpy})_2(N_3)_2]_n$ (**2**), and *cis*-$[Mn(3,5lut)_2(N_3)_2]_n$ (**3**) were structurally characterized. The three compounds

* To whom correspondence should be addressed. E-mail: aescuer@kripto.qui.ub.es.
[†] Alexandria University.
[‡] Universitat de Barcelona.
[§] Università degli Studi di Firenze.
[||] Kuwait University.
[⊥] Technische Universität Graz.

(1) Goher, M. A. S.; Mautner, F. A. *Croat. Chem. Acta* **1990**, *63*, 559.
(2) Escuer, A.; Vicente, R.; Goher, M. A. S.; Mautner, F. A. *Inorg. Chem.* **1996**, *35*, 6386.
(3) Escuer, A.; Vicente, R.; Mautner, F. A.; Goher, M. A. S. *Inorg. Chem.* **1997**, *36*, 3440.
(4) Escuer, A.; Vicente, R.; Goher, M. A. S.; Mautner, F. A. *Inorg. Chem.* **1995**, *34*, 5707.
(5) Escuer, A.; Vicente, R.; Goher, M. A. S.; Mautner, F. A. *J. Chem. Soc., Dalton Trans.* **1997**, 4431.
(6) Goher, M. A. S.; Al-Salem, N. A.; Mautner, F. A. *J. Coord. Chem.* **1998**, *44*, 119.
(7) Escuer, A.; Vicente, R.; Goher, M. A. S.; Mautner, F. A. *Inorg. Chem.* **1998**, *37*, 782.
(8) Abu-Youssef, M.; Escuer, A.; Goher, M. A. S.; Mautner, F. A.; Vicente, R. *Eur. J. Inorg. Chem.* **1999**, 687.
(9) Shen, H. Y.; Liao, D. Z.; Jiang, Z. H.; Yan, S. P.; Sun, B. W.; Wang, G. L.; Yao, X. K.; Wang, H. G. *Chem. Lett.* **1998**, 469.
(10) (a) De Munno, G.; Julve, M.; Viau, G.; Lloret, F.; Faus, J.; Viterbo, D. *Angew. Chem., Int. Ed. Engl.* **1996**, *35*, 1807. (b) Cortés, R.; Lezama, L.; Pizarro, J. L.; Arriortua, M. I.; Rojo, T. *Angew. Chem., Int. Ed. Engl.* **1996**, *35*, 1810.
(11) (a) Cortés, R.; Pizarro, J. L.; Lezama, L.; Arriortua, M. I.; Rojo, T. *Inorg. Chem.* **1994**, *33*, 2697. (b) During the refereeing process, a compound similar to **1**, was published: Manson, J. L.; Arif, A. M.; Miller, J. S. *Chem. Commun.* **1999**, 1479.

10.1021/ic990656x CCC: $18.00
Published on Web 11/23/1999

consist of well-isolated chains in which the manganese atoms are bridged by two azido ligands, in the EO mode for **1**, alternating EO−EE modes for **2**, and EE mode for **3**, showing the expected ferromagnetic (**1**), alternating ferro−antiferromagnetic (**2**), and antiferromagnetic (**3**) coupling. It should be underlined that compound **1** is the first example[11b] characterized to date of one-dimensional manganese−azido systems with only EO bridges. These systems are almost ideal for the investigation of spin dynamics via EPR spectroscopy. In fact they provide the possibility of finding all the features of a quasi-ideal Heisenberg system and enable the response of unprecedented manganese ferromagnetic and alternated ferro−antiferromagnetic systems to be explored.

In this paper we present the synthesis, structural characterization, magnetic behavior, and selected EPR data (mainly room-temperature measurements) of these fascinating new one-dimensional systems.

Experimental Section

$[Mn(2\text{-}Bzpy)(N_3)_2]_n$ (1) was synthesized by mixing an aqueous−methanolic solution (1:1, 20 mL) of manganese(II) nitrate tetrahydrate (1.00 g, ca. 4 mmol) and 1.83 g (ca. 10 mmol) of 2-benzoylpyridine dissolved in 15 mL of methanol, followed by dropwise addition of a concentrated aqueous solution of sodium azide (0.65 g, 10 mmol). The resulting yellow-brown mixture was left to stand in a desiccator in a dark place for several weeks to form long deep red crystals of **1** suitable for X-ray determination; yield, ca. 75%. Anal. Calcd for $MnC_{12}H_9N_7O$: C, 44.74; H, 2.82; N, 30.43; Mn, 17.05. Found: C, 44.5; H, 2.7; N, 30.5; Mn, 17.0.

$[Mn(3\text{-}Bzpy)_2(N_3)_2]_n$ (2) was synthesized by mixing an aqueous−methanolic solution (1:1, 30 mL) of manganese(II) chloride tetrahydrate (0.59 g, 3 mmol) and 1.10 g (ca. 6 mmol) of 3-benzoylpyridine dissolved in 20 mL of methanol, followed by dropwise addition of a concentrated aqueous solution of sodium azide (0.65 g, 10 mmol). A few drops of L-ascorbic acid in methanol were added to the resulted yellow mixture in order to prevent oxidation of Mn(II). The clear solution was left to stand in a dark place for several days to form light yellow platelike crystals of **2** suitable for X-ray determination; yield, ca. 60%. Anal. Calcd for $MnC_{24}H_{18}N_8O_2$: C, 57.04; H, 3.59; N, 22.17; Mn, 10.87. Found: C, 56.9; H, 3.5; N, 22.3; Mn, 10.7.

$[Mn(3,5\text{-}lutidine)_2(N_3)_2]_n$ (3) was prepared in the same way as compound **1** but using the following quantities of the starting reagents: 1.00 g (4 mmol) of manganese(II) nitrate tetrahydrate, 1.07 g (10 mmol) of 3,5-lutidine, and 0.65 g (10 mmol) of sodium azide. The resulting solution was kept in the dark for about 2 weeks to yield large well-formed greenish-yellow crystals of compound **3**; yield, ca. 70%. Anal. Calcd for $MnC_{14}H_{18}N_8$: C, 47.60; H, 5.14; N, 31.72; Mn, 15.55. Found: C, 47.7; H, 5.2; N, 31.5; Mn, 15.6.

Spectral and Magnetic Measurements. Infrared spectra (400−4000 cm^{-1}) were recorded from KBr pellets on a Nicolet 520 FTIR spectrophotometer. Magnetic measurements were carried out with a DSM8 pendulum susceptometer, working in the temperature range 300−4 K. The applied external magnetic field was 1.5 T. Magnetic measurements on the ferromagnetic compound **1** were performed with a Quantum Desing instrument with a SQUID detector, working in the temperature range 300−2 K under an external magnetic field of 100 G. Diamagnetic corrections were estimated from Pascal tables. EPR spectra were recorded at X-band frequency with a Bruker ES200 spectrometer equipped with an Oxford liquid helium cryostat for variable-temperature work.

Crystal Structure Analysis of 1−3. The X-ray single-crystal data for the three compounds were collected on a modified STOE four-circle diffractometer. The crystal sizes of **1**−**3**, respectively, are as follows: 0.55 × 0.28 × 0.22; 0.44 × 0.40 × 0.30; and 0.47 × 0.25 × 0.25 mm. The crystallographic data, conditions retained for the intensity data collection, and some features of the structure refinements are listed in Table 1. Graphite-monochromatized Mo Kα radiation (λ = 0.710 69 Å) with the ω-scan technique was used to collect the data sets. The accurate unit-cell parameters of **1**−**3** were determined from automatic centering of 36 reflections (8.9° < θ < 15.3°), 33 reflections (8.0° < θ < 19.0°), and 55 reflections (7.5° < θ < 14.9°) and refined by least-squares methods; 8230 reflections (7085 independent reflections, R_{int} = 0.0386), 4921 reflections (4229 independent reflections; R_{int} = 0.0299), and 4569 reflections (3685 independent reflections; R_{int} = 0.0320) were collected in the ranges 2.75° < θ < 26.00°, 2.90° < θ < 26.00°, and 2.92° < θ < 27.99°. Intensity decays of 12, 2, and 3% for control reflections (2 0 0; 0−3 3; 3 2−3), (1−1−6; 3 1−1; 2−2 1), and (−2−1 2; 0 3 2), measured after every set of 100 reflections, were observed during data collection. Corrections were applied for Lorentz−polarization effects, for intensity decay, and for absorption using the DIFABS[12] computer program. The structures were solved by Patterson and direct methods using the SHELXS-86[13] computer program, and refined by full-matrix least-squares methods on F^2 (i.e. squared), using the SHELXL-93[14] program incorporated in the SHELXTL/PC V 5.03[15] program library and the graphics program PLUTON.[16] All non-hydrogen atoms were refined anisotropically. The hydrogen atoms were fixed geometrically with the HFIX utility.[15] Final R factors for all observed reflections are 0.0669, 0.0555, and 0.0617; the number of refined parameters are 568, 320, and 212, respectively. Maximum and minimum peaks in the final difference synthesis are as follows: 0.570 and −0.745 e $Å^{-3}$, 0.209 and −0.218 e $Å^{-3}$, and 0.299 and −0.440 e $Å^{-3}$. Significant bond parameters for **1**−**3** are given in Tables 2−4, respectively.

Table 1. Crystal Data and Structure Refinement for $[Mn(2\text{-}Bzpy)(N_3)_2]_n$ (**1**), $[Mn(3\text{-}Bzpy)_2(N_3)_2]_n$ (**2**), and $[Mn(3,5\text{-}lut)_2(N_3)_2]_n$ (**3**)

	1	**2**	**3**
chem formula	$C_{12}H_9MnN_7O$	$C_{24}H_{18}MnN_8O_2$	$C_{14}H_{18}MnN_8$
formula weight	322.20	505.40	353.30
space group	$P2_1/n$	$C2/c$	$P2_1/n$
a, Å	14.413(4)	14.179(5)	13.552(6)
b, Å	16.157(4)	9.698(4)	7.730(3)
c, Å	18.478(5)	34.351(12)	16.554(6)
α, deg	90.0	90.0	90.0
β, deg	96.77(3)	97.81(3)	101.69(3)
γ, deg	90.0	90.0	90.0
V, $Å^3$	4273(2)	4680(3)	1698.2(12)
Z	12	8	4
T, K	293(2)	295(2)	295(2)
λ(Mo Kα), Å	0.710 69	0.710 69	0.710 69
d_{calc}, $Mg\cdot m^{-3}$	1.503	1.435	1.382
μ(Mo Kα), mm^{-1}	0.936	0.603	0.789
R^a	0.0669	0.0555	0.0617
$R_w{}^{2\,b}$	0.1501	0.0928	0.1225

[a] $R(F_o) = \sum F_o - F_c/\sum F_o$. [b] $(R_w(F_o)^2 = \{\sum[w((F_o)^2 - (F_c)^2)^2]/\sum[w((F_o)^2)^2]\}^{1/2}$.

Results and Discussion

Description of the Structure of *cis*-$[Mn(2\text{-}bzpy)(N_3)_2]_n$ (1). An ORTEP plot of the basic unit of $[Mn(2\text{-}bzpy)(N_3)_2]_n$ is shown in Figure 1a. The structure consists of neutral chains of manganese atoms linked by EO azido bridges along the (0 0 1) direction, Figure 1b. The manganese atoms are octahedrally coordinated by a chelating 2-benzoylpyridine and four azido ligands which act as end-on double bridges with the two neighboring manganese ions. The azido ligands are linear and show asymmetric N−N distances, close to 1.20/1.14 Å. Three different manganese atoms, Mn(1), Mn(2), and Mn(3), may be

(12) Walker, N.; Stuart, D. *Acta Crystallogr*. **1983**, *A39*, 158.
(13) Sheldrick, G. M. *SHELXS-86, Program for the Solution of Crystal Structure*; University of Gottingen: Gottingen, Germany, 1986.
(14) Sheldrick, G. M. *SHELXL-93, Program for the Refinement of Crystal Structure*; University of Gottingen: Gottingen, Germany, 1993.
(15) *SHELXTL 5.03 (PC Version), Program Library for the Solution and Molecular Graphics*; Siemens Analytical Instruments Division: Madison, WI, 1995.
(16) Spek, A. L. *PLUTON-92*; University of Utrecht: Utrecht, The Netherlands, 1992.

Table 2. Selected Bond Lengths (Å) and Angles (deg) for **1**

Mn(1)−O(1)	2.308(3)	Mn(2)−O(2)	2.278(3)
Mn(1)−N(1)	2.305(4)	Mn(2)−N(2)	2.275(4)
Mn(1)−N(11)	2.220(4)	Mn(2)−N(11)	2.176(4)
Mn(1)−N(21)	2.197(4)	Mn(2)−N(21)	2.239(4)
Mn(1)−N(41)	2.176(4)	Mn(2)−N(31)	2.200(4)
Mn(1)−N(51)	2.205(4)	Mn(2)−N(31a)	2.201(4)
Mn(3)−O(3)	2.286(3)		
Mn(3)−N(3)	2.265(4)	Mn(1)···Mn(2)	3.396(1)
Mn(3)−N(41)	2.233(4)	Mn(1)···Mn(3)	3.386(1)
Mn(3)−N(51)	2.198(4)	Mn(2)···Mn(2a)	3.364(1)
Mn(3)−N(61)	2.203(4)	Mn(3)···Mn(3b)	3.415(1)
Mn(3)−N(61b)	2.204(4)		

O(1)−Mn(1)−N(1)	70.6(1)	N(21)−Mn(2)−N(31)	97.5(1)
O(1)−Mn(1)−N(11)	93.7(1)	N(21)−Mn(2)−N(31a)	173.9(1)
O(1)−Mn(1)−O(21)	162.1(1)	N(31)−Mn(2)−N(31a)	80.3(2)
O(1)−Mn(1)−O(41)	90.7(1)	O(3)−Mn(3)−N(3)	70.5(1)
O(1)−Mn(1)−O(51)	86.7(1)	O(3)−Mn(3)−N(41)	84.8(1)
N(1)−Mn(1)−N(11)	87.1(1)	O(3)−Mn(3)−N(51)	91.6(1)
N(1)−Mn(1)−N(21)	92.3(1)	O(3)−Mn(3)−N(61)	96.6(1)
N(1)−Mn(1)−N(41)	100.5(1)	O(3)−Mn(3)−N(61b)	163.7(1)
N(1)−Mn(1)−N(51)	157.3(1)	N(3)−Mn(3)−N(41)	154.7(2)
N(11)−Mn(1)−N(21)	79.5(1)	N(3)−Mn(3)−N(51)	95.6(1)
N(11)−Mn(1)−N(41)	172.1(1)	N(3)−Mn(3)−N(61)	92.7(2)
N(11)−Mn(1)−N(51)	93.7(1)	N(3)−Mn(3)−N(61b)	94.0(2)
N(21)−Mn(1)−N(41)	98.2(1)	N(41)−Mn(3)−N(51)	78.9(1)
N(21)−Mn(1)−N(51)	110.1(2)	N(41)−Mn(3)−N(61)	95.9(1)
N(41)−Mn(1)−N(51)	80.0(1)	N(41)−Mn(3)−N(61b)	111.0(1)
O(2)−Mn(2)−N(2)	70.4(1)	N(51)−Mn(3)−N(61)	169.8(2)
O(2)−Mn(2)−N(11)	163.1(1)	N(51)−Mn(3)−N(61b)	95.2(1)
O(2)−Mn(2)−N(21)	92.2(1)	N(61)−Mn(3)−N(61b)	78.4(2)
O(2)−Mn(2)−N(31)	85.2(1)	Mn(1)−N(11)−Mn(2)	101.1(2)
O(2)−Mn(2)−N(31a)	93.2(1)	Mn(1)−N(21)−Mn(2)	99.9(2)
N(2)−Mn(2)−N(11)	94.8(1)	Mn(1)−N(41)−Mn(3)	100.3(2)
N(2)−Mn(2)−N(21)	90.5(1)	Mn(1)−N(51)−Mn(3)	100.5(2)
N(2)−Mn(2)−N(31)	154.6(1)	Mn(2)−N(31)−Mn(2a)	99.7(2)
N(2)−Mn(2)−N(31a)	93.9(1)	Mn(3)−N(61)−Mn(3b)	101.6(2)
N(11)−Mn(2)−N(21)	79.5(1)		
N(11)−Mn(2)−N(31)	110.3(2)	Mn(1)···Mn(2)···Mn(2a)	132.52(4)
N(11)−Mn(2)−N(31a)	95.9(1)	Mn(1)···Mn(3)···Mn(3b)	127.88(4)
		Mn(2)···Mn(1)···Mn(3)	132.38(3)

Table 3. Selected Bond Lengths (Å) and Angles (deg) for **2**

Mn(1)−N(1)	2.308(3)	Mn(1)−N(2)	2.264(3)
Mn(1)−N(11)	2.229(3)	Mn(1)−N(11a)	2.219(3)
Mn(1)−N(21)	2.235(3)	Mn(1)−N(23b)	2.244(3)

N(1)−Mn(1)−N(2)	172.6(1)	N(11)−Mn(1)−N(11a)	79.6(1)
N(1)−Mn(1)−N(11)	94.7(1)	N(11)−Mn(1)−N(21)	91.0(1)
N(1)−Mn(1)−N(11a)	92.1(1)	N(11)−Mn(1)−N(23b)	173.9(1)
N(1)−Mn(1)−N(21)	86.0(1)	N(11a)−Mn(1)−N(21)	170.3(1)
N(1)−Mn(1)−N(23b)	85.8(1)	N(11a)−Mn(1)−N(23b)	94.3(1)
N(2)−Mn(1)−N(11)	92.6(1)	N(21)−Mn(1)−N(23b)	95.1(1)
N(2)−Mn(1)−N(11a)	90.6(1)	Mn(1)−N(11)−Mn(1a)	100.4(1)
N(2)−Mn(1)−N(21)	92.4(1)	N(22)−N(21)−Mn(1)	126.0(2)
N(2)−Mn(1)−N(23b)	87.1(1)	N(22)−N(23)−Mn(1b)	126.1(2)

found along the chain, which, combined with the inversion centers placed between Mn(2)−Mn(2A) and Mn(3)−Mn(3A) and the absence of an inversion center on Mn(1), give rise to the Mn(3)−Mn(1)−Mn(2)−Mn(2A)−Mn(1A)−Mn(3A)−Mn(3B) sequence with four different bridges between them. Bond angles in the two centrosymmetric Mn(2)−N(31)−Mn(2A) and Mn(3)−N(61)−Mn(3B) units are 99.7(2) and 101.6(2)°, respectively, whereas the bond angles for the remaining noncentrosymmetric units are Mn(3)−N(41)−Mn(1) and Mn(3)−N(51)−Mn(1) 100.3(2) and 100.5(2)°, and Mn(1)−N(11)−Mn(2) and Mn(1)−N(21)−Mn(2), 101.1(2) and 99.9(2)°. The four different Mn···Mn distances range between 3.364(1) and 3.415(1) Å. The chains are well-isolated due to the large 2-bzpy ligand, the minimum Mn···Mn interchain distance being 9.931(1) Å. Dihedral angles between neighboring Mn_2N_2 rings are close to 90° due to the cis coordination, whereas they are roughly coplanar with the corresponding next-nearest-neighbor rings along the chain.

Table 4. Selected Bond Lengths (Å) and Angles (deg) for **3**

Mn(1)−N(1)	2.251(3)	Mn(1)−N(2)	2.271(3)
Mn(1)−N(11)	2.225(3)	Mn(1)−N(13a)	2.252(3)
Mn(1)−N(21)	2.220(3)	Mn(1)−N(23b)	2.245(3)

N(1)−Mn(1)−N(2)	99.3(1)	N(11)−Mn(1)−N(21)	173.4(1)
N(1)−Mn(1)−N(11)	87.3(1)	N(11)−Mn(1)−N(23b)	89.4(1)
N(1)−Mn(1)−N(13a)	89.1(1)	N(13a)−Mn(1)−N(21)	90.1(1)
N(1)−Mn(1)−N(21)	88.5(1)	N(13a)−Mn(1)−N(23b)	85.0(1)
N(1)−Mn(1)−N(23b)	173.0(1)	N(21)−Mn(1)−N(23b)	95.3(1)
N(2)−Mn(1)−N(11)	88.8(1)	N(12)−N(11)−Mn(1)	121.9(3)
N(2)−Mn(1)−N(13a)	171.0(1)	N(12)−N(13)−Mn(1b)	125.8(3)
N(2)−Mn(1)−N(21)	86.8(1)	N(22)−N(21)−Mn(1)	122.9(3)
N(2)−Mn(1)−N(23b)	86.8(1)	N(22)−N(23)−Mn(1b)	124.8(3)
N(11)−Mn(1)−N(13a)	94.9(1)		

Description of the Structure of *trans*-[Mn(3-Bzpy)$_2$(N$_3$)$_2$]$_n$ (2). The structure of **2** is shown in Figure 2a. It consists of octahedrally coordinated manganese atoms in which the coordination sites are occupied by two 3-benzoylpyridine ligands in trans arrangement and four azido ligands which form double bridges between neighboring manganese ions. The azido groups in the double bridges are alternately in the EE and EO modes, giving an alternating chain, Figure 2a. The EO azido bridges show asymmetric N−N distances of 1.182(4)/1.157(4) Å, whereas the EE bridges are more symmetric, 1.178(4)/1.169(4) Å. The $Mn_2(\mu_{1,3}\text{-}N_3)_2$ ring is quite regular: bond lengths are Mn(1)−N(21) = 2.235(3) Å and Mn(1)−N(23b) = 2.244(3) Å, and bond angles are Mn(1)−N(21)−N(22) = 126.0(2)° and Mn(1)−N(23b)−N(22)b = 126.1(2)°. The Mn−$(\mu_{1,3}\text{-}N_3)_2$−Mn ring shows the typical distortion from the planar to the chair conformation, evaluated as a δ parameter[7] = 26.6(1)°. The centrosymmetric Mn_2N_2 ring is strictly planar, as is usual for double end-on bridges, and shows a bond angle Mn(1)−N(11)−Mn(1)a = 100.4(1)° and bond lengths Mn(1)−N(11) and Mn(1)−N(11)a of 2.229(3) and 2.219(3) Å, respectively. The Mn···Mn distances are asymmetric, the longer corresponding to the EE ring, Mn(1)−Mn(1)b = 5.229(2) Å, and the shorter to the EO ring, Mn(1)−Mn(1)a = 3.416(2) Å.

The N(1)−Mn(1)−N(2) bond angle of the axial pyridine ligands is 172.6(1)°. This deviation from 180° has the effect of moving away the axial ligands on the EO ring. In contrast, the shortest contact between the benzoyl groups, smaller than 4 Å, was found between the ligands on the EE rings.

The packing of the chains shows an unusual feature: the chains are placed along the 1 1 0 and 1 −1 0 directions in pseudoplanes of parallel chains, Figure 2b. The parallel chains are well-isolated by the pyridine ligands, allowing minimum Mn···Mn interchain distances of 7.753(3) Å, whereas the minimum Mn···Mn distance between the pseudoplanes placed at 0, $^1/_2$ and 1 in the *z* direction is greater than 17 Å, as a consequence of the trans coordination of the 3-bzpy rings along the *z* axis.

Description of the Structure of *cis*-[Mn(3,5lut)$_2$(N$_3$)$_2$]$_n$ (3). An ORTEP plot of *cis*-[Mn(3,5lut)$_2$(N$_3$)$_2$]$_n$ is shown in Figure 3a. The structure consists of neutral chains of manganese atoms linked by azido bridges, placed along the (0 1 0) direction, Figure 3b. In this case the octahedral coordination around the manganese atoms consists of two 3,5-dimethylpyridine ligands coordinated by means of the pyridine nitrogen atom and four azido bridges which act as EE double bridges with the two neighboring manganese ions. The two sets of EE bridges are not equivalent, giving an alternating system. In this case, the N−N bond distances are practically symmetrical, around 1.70 Å. The bond angles Mn(1)−N(11)−N(12) and Mn(1)−N(13A)−

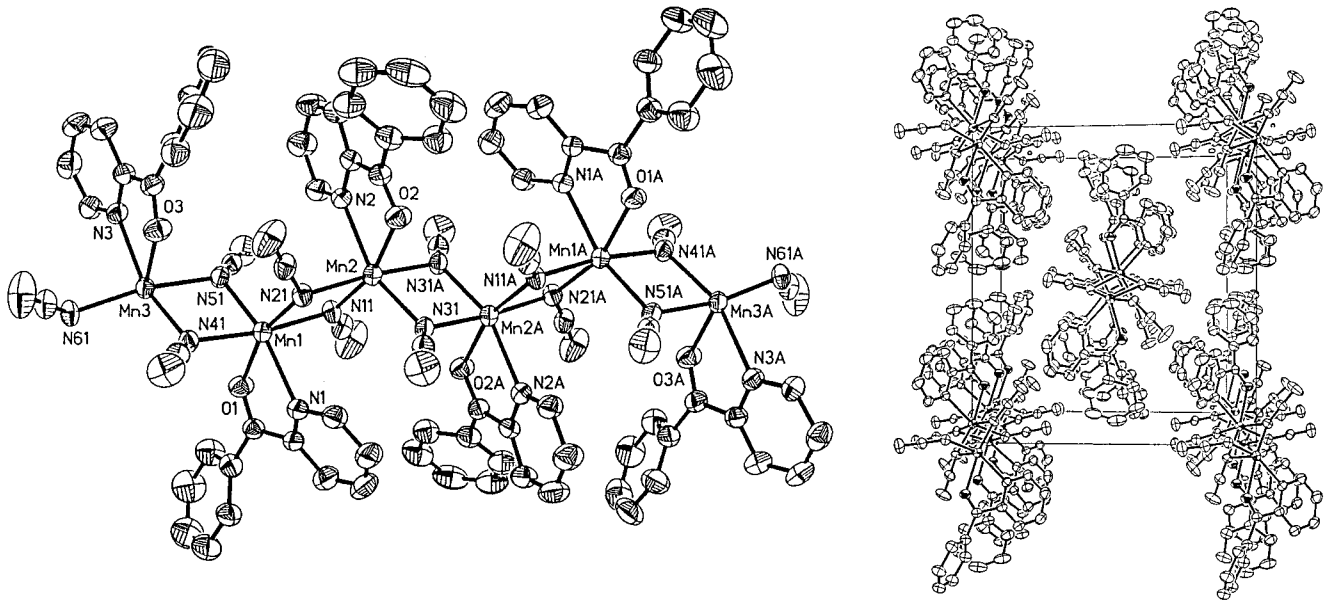

Figure 1. (a, left) ORTEP drawing for *cis*-[Mn(2-bzpy)$(N_3)_2]_n$ (**1**). Ellipsoids at the 50% probability level. (b, right) Packing of the well-isolated chains along the *c* axis.

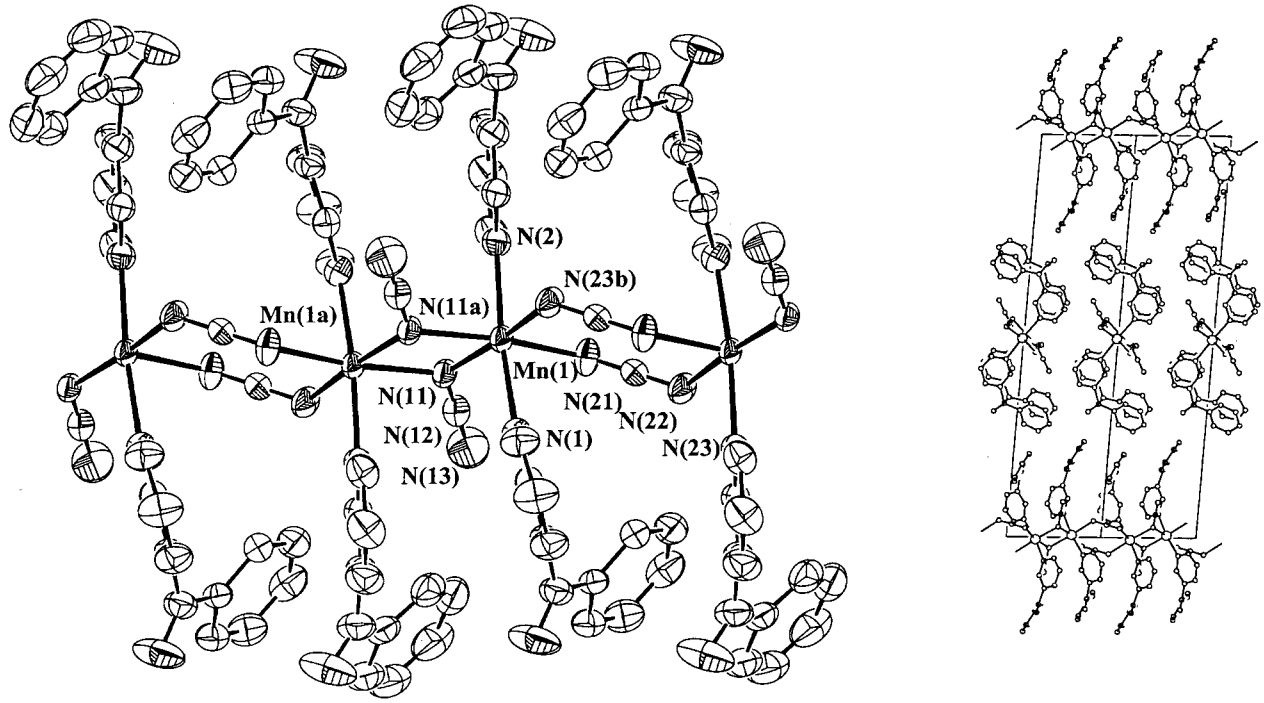

Figure 2. (a, left) ORTEP drawing for *trans*-[Mn(3-bzpy)$_2(N_3)_2]_n$ (**2**). Ellipsoids at the 50% probability level. (b, right) View of the packing along the (110) direction showing the different orientations of the chains placed at $z = 1$ and 0 from those at $z = {}^1/_2$ and the large interchain distance (>17 Å) along the *c* axis.

N(12A), 121.9(2) and 125.8(2)°, Mn(1)−N(21)−N(22) and Mn(1)−N(23B)−N(22B), 122.9(3) and 124.8(3)°, lie in the normal range[5] found for related EE compounds. Deviation from planarity to chair conformation for the $Mn(N_3)_2Mn$ eight-membered rings, measured as the δ torsion angle between the plane defined by the six N coplanar atoms of the bridges and the corresponding N−Mn−N planes, takes the δ_A 32.7(1) and δ_B 31.6(1)° values with the corresponding manganese atoms deviating 0.818(1) and 0.788(1) Å from A and B planes. Mn···Mn intrachain distances are 5.159(1) and 5.140(1) Å for A and B rings, respectively, whereas the minimum interchain distance is 9.277(1) Å due to the large size of the lutidine ligands which efficiently isolate the chains. It is worth pointing out that the manganese skeleton consists of a zigzag chain due to the cis coordination of the bridges with a Mn(1A)···Mn(1)···Mn(1B) angle of 97.28(3)°, Figure 3a.

Magnetic Susceptibility and Powder EPR Spectra. The $\chi_M T$ product vs *T* for **1** measured with a low external field (100 G) shows a continuous increase from the room-temperature value (4.39 $cm^3 \cdot K \cdot mol^{-1}$) down to 2 K, where it reaches the value of 32.8 $cm^3 \cdot K \cdot mol^{-1}$, Figure 4. This plot indicates weak ferromagnetic coupling, with no evidence of interchain interactions, which is consistent with the large interchain distance. According to the structural data, compound **1** shows a compli-

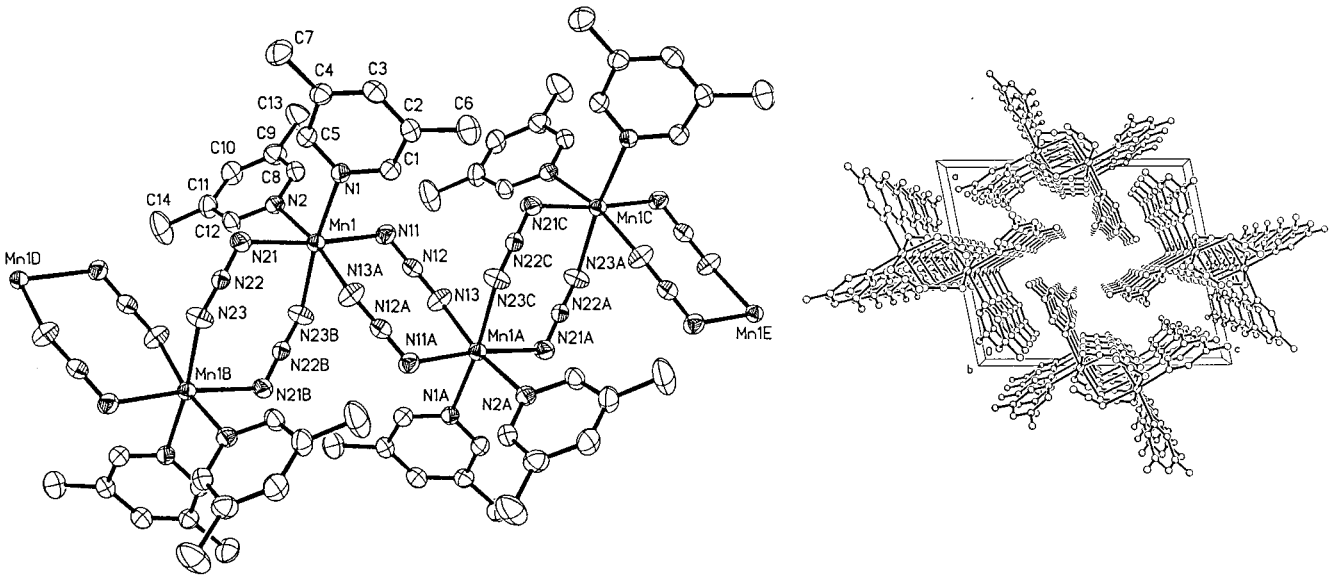

Figure 3. (a, left) ORTEP drawing for *cis*-$[Mn(35lut)_2(N_3)_2]_n$ (**3**). Ellipsoids at the 50% probability level. (b, right) Packing of the well-isolated chains along the *b* axis.

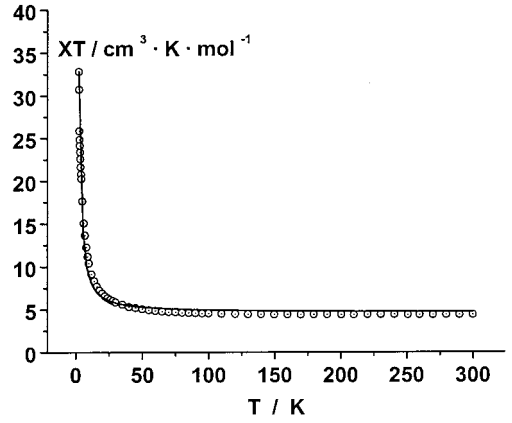

Figure 4. Plot of the $\chi_M T$ product vs T for *cis*-$[Mn(2\text{-}bzpy)(N_3)_2]_n$ (**1**). Solid line shows the best fit of the data (see text).

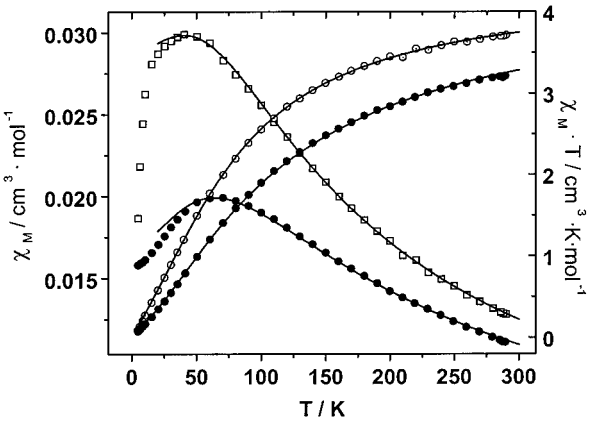

Figure 5. Plot of the molar susceptibility and $\chi_M T$ product vs T for *trans*-$[Mn(3\text{-}bzpy)_2(N_3)_2]_n$ (**2**) (open symbols) and *cis*-$[Mn(35lut)_2(N_3)_2]_n$ (**3**) (filled symbols). Solid lines show the best fit of the data (see text).

cated alternance of coupling constants Mn3′−(J1)−Mn1′−(J2)−Mn2′−(J3)−Mn2−(J2)−Mn1−(J1)−Mn3−(J4)−Mn3″. No model is available for fitting the temperature dependence of χT for such complex systems, but, given the similar Mn−N−Mn bond angles for the different bridges along the chain, the coupling was evaluated as an average value using the conventional equations[17] derived by Fisher for the magnetic susceptibility of an infinite chain of classical spins based on the Hamiltonian $H = -J\sum S_i S_{i+1}$ for local spin values $S = {}^5/_2$ with one J parameter. The best-fit parameters are $J = +0.80(2)$ cm^{-1}, $g = 2.05(1)$. The magnetization measured at 2.5 K reaches 4.3 μ_B at 5 T, showing that under these conditions the magnetization is not yet saturated.

Compound 2. The χT vs T plot in the 300−4 K range is shown in Figure 5. The overall behavior indicates a dominant antiferromagnetic interaction, with a room-temperature $\chi_M T$ value of 3.70 cm^3·K·mol^{-1}, which decreases continuously and tends to zero when the temperature decreases. χ_M shows a broad maximum centered at 40 K. The magnetic data were analyzed by means of the reported expression[18] derived from the Hamiltonian $H = -J_1\sum S_{2i}S_{2i+1} - J_2\sum S_{2i}S_{2i+2}$, and the best-fit parameters were $J_1 = -12.31(3)$ cm^{-1}, $J_2 = +3.5(3)$ cm^{-1}, and $g = 1.99(1)$. This result compares well with results reported for similar alternating compounds with ferro−antiferromagnetic interactions such as $[Mn(bpy)(N_3)_2]_n$ for which[18] J_1 was −11.8 cm^{-1} and J_2 was +9.6 cm^{-1}, or the more recent $[Mn(3\text{-}Et,4\text{-}Mepy)_2(N_3)_2]_n$ compound for which[8] J_1 was −13.7 cm^{-1} and J_2 was +2.4 cm^{-1}.

Compound 3. The plot of the magnetic data in the 300−4 K range is shown in Figure 5. The general behavior corresponds to an antiferromagnetically coupled system, with a room-temperature $\chi_M T$ value of 3.21 cm^3·K·mol^{-1}, which decreases continuously and tends to zero when the temperature decreases. χ_M shows a broad maximum at 70 K. Fit of the susceptibility data was performed with the Fisher equation,[17] Hamiltonian $H = -J\sum S_i S_{i+1}$, and the best-fit parameters were $J = -10.59(4)$ cm^{-1} and $g = 2.007(3)$. In this case, the results are also comparable to those obtained for related compounds[7] such as $[Mn(pyOH)_2(N_3)_2]_n$ ($J = -7.0$ cm^{-1}) or $[Mn(3Etpy)_2(N_3)_2]_n$ ($J = -13.8/-11.7$ cm^{-1}) with comparable chair distortions in the bridge region.

The room-temperature polycrystalline powder X-band EPR spectrum for **1** shows a broad band with a peak-to-peak width

(17) Fisher, M. E. *Am. J. Phys.* **1964**, *32*, 343.
(18) Cortés, R.; Drillon, M.; Solans, X.; Lezama, L.; Rojo, T. *Inorg. Chem.* **1997**, *36*, 677.

$\Delta H_{pp} = 750$ G centered at $g = 2.05$, confirming well the g value obtained from susceptibility measurements. However, the spectrum of **3** shows a very sharp line $\Delta H_{pp} = 40$ G centered at $g = 2.00$ and a weak half-field signal at $g = 4.00$, whereas **2** shows a line with $\Delta H_{pp} = 220$ G centered at $g = 2.02$. The line width of the spectra of one-dimensional compounds is the result of two conflicting contributions: intrachain superexchange interactions which tend to narrow the lines and dipolar interactions which tend to broaden them.[19] The exchange coupling constants in **2** and **3** are of the same order, while that in **1** is an order of magnitude smaller. The dipolar interactions are mainly determined by the Mn−Mn distance: the shorter the distance the stronger the interaction. In qualitative terms exchange narrowing becomes dominant for **3**, in which the Mn···Mn distances are relatively long, 5.159 and 5.140 Å, and the J value is relatively high (-10.59 cm^{-1}). In contrast **1**, which shows very short Mn···Mn distances of 3.364 and 3.414 Å, and a low J value (less than 1 cm^{-1}), has the broadest line. The intermediate line width value obtained for the alternating chain **2** is consistent with the alternating short−long Mn···Mn distances (5.229 and 3.416 Å), and J values comparable to **1** and **3** offer the mixing of the two opposite effects. These results are also comparable to those obtained for the alternating EE/EO systems $[Mn(bpy)(N_3)_2]_n$ [18] or $[Mn(3Et,4Mepy)(N_3)_2]_n$ [8] which show line widths of 500 and 320 G, respectively, and the EE bridged systems $[Mn(L)_2(N_3)_2]_n$, L = pyOH or 3-Etpy, with line widths of 35−42 G.[7]

Variable-temperature EPR spectra show common features for **1**−**3**: the line width decreases slightly when T decreases, and at low temperatures, between 100 and 4 K, a significant broadening of the signal was observed, reaching values close to 2000 G for **1**, 750 G for **2**, and 1300 G for **3** as a consequence of the increased correlations along the chain. In addition, compounds **1** and **3** show new signals giving a complicated pattern, probably due to the anisotropic shift of the signals expected at low T.

Single-Crystal EPR Experiments. EPR properties of manganese quasi-ideal Heisenberg 1-D antiferromagnets have been studied for several systems, mainly for $[(CH_3)_4N)][MnCl_3]$ (TMMC).[19] On the basis of the structural data and of the variation of the line width observed in the powder EPR spectra for **1**−**3**, single-crystal measurements were performed, to characterize in more detail the spin dynamics in systems with different kinds of magnetic interactions and to estimate the intrachain to the interchain exchange interaction.

(a) *cis*-[Mn(2-bzpy)(N$_3$)$_2$]$_n$ (1). For the single-crystal experiments a well-formed prismatic crystal in which the chain direction corresponds to the elongation axis of the prism was used. The spectra were recorded by rotating around the perpendiculars in the chain direction. A third rotation around the chain direction was also performed. The first rotations were practically identical to each other, and the angular dependence of the peak-to-peak width ΔH_{pp} for one of them is shown in Figure 6. Maximum broadening was found in the parallel direction, $\Delta H_{pp} = 2095$ G; a well-defined minimum in the line width was found at the magic angle $\theta = 54.7°$, $\Delta H_{pp} = 500$ G, and a local maximum along the direction perpendicular to the chain, $\Delta H_{pp} = 760$ G. This is the expected behavior for one-dimensional magnets in which spin diffusion determines a large secular enhancement.[19−21] The dependence of the line width is consistent with the $\Delta H_{pp} = a + b(3\cdot\cos^2\theta - 1)^{4/3}$, as expected.[19] The best fit values are $a = 309$ G, $b = 639$ G. A further confirmation of the one-dimensional behavior comes from the analysis of the line shape which is Lorentzian at the magic angle. Some deviation from this is observed at $\theta = 90°$, and it is diffusive at $\theta = 0°$. The rotation around the chain axis shows only a minor variation in the line width in the 180° rotation (100 G approximately), Figure 6. The important information which emerges from the EPR spectra is linked to the fact that the line shape, following the characteristic one-dimensional behavior, provides an upper limit[22] to the interchain exchange interactions, J', which would restore the Lorentzian line shape as $J'/J \leq 10^{-3}$.

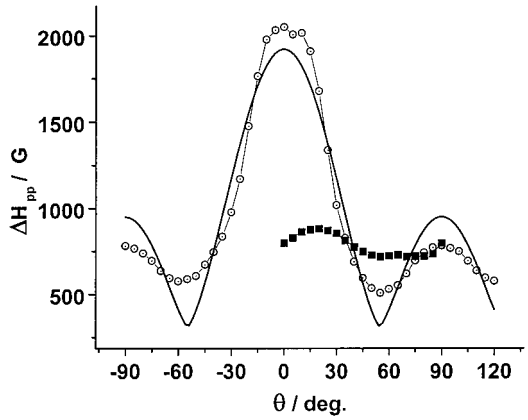

Figure 6. Angular dependence of the peak-to-peak line width ΔH_{pp} of *cis*-$[Mn(2\text{-}bzpy)(N_3)_2]_n$ (**1**) at room temperature and X-band. Dot-centered circles show the dependence of ΔH_{pp} between the parallel ($\theta = 0°$) and the perpendicular ($\theta = 90°$) orientations of the external field with the chain axis c. The solid line shows the expected angular dependence $[3\cos^2\theta - 1]^{4/3}$. Filled squares are ΔH_{pp} for a constant $\theta = 90°$ rotation.

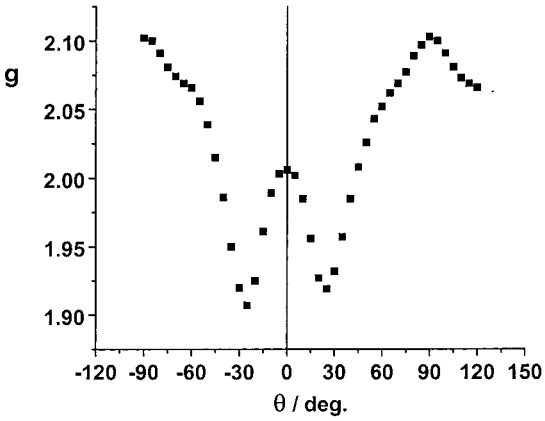

Figure 7. Angular dependence of the g value *cis*-$[Mn(2\text{-}bzpy)(N_3)_2]_n$ (**1**) at room temperature and X-band.

The g parameter was also checked along the rotation, from the observation of the anomalous g value of 2.05 found from susceptibility or powder EPR spectra. The g dependence vs θ is plotted in Figure 7, which shows a maximum of $g = 2.10$ at $\theta = 90°$, $g = 2.01$ for $\theta = 0°$ and a minimum value of 1.91 for $\theta = 25°$. Similar behavior was observed in several compounds, such as in $[Cu(hfac)_2(NITMe)]$,[23] a ferromagnetic Cu(II)-radical

(19) Bencini, A.; Gatteschi, D. *EPR of Exchange Coupled Systems*; Springer-Verlag: Berlin, Heidelberg 1990, Chapter 10, and references cited therein.

(20) Kalt, H.; Siegel, E.; Pauli, N.; Mosebach, H.; Wiese, J.; Edgar, A. *J. Phys. C* **1983**, *16*, 6427.

(21) Richards, P. M.; Quinn, R. K.; Morosin, B. *J. Chem. Phys.* **1973**, *59*, 4474.

(22) Hennessy, M. J.; McElwee, C. D.; Richards, P. M. *Phys. Rev. B* **1973**, *7*, 930.

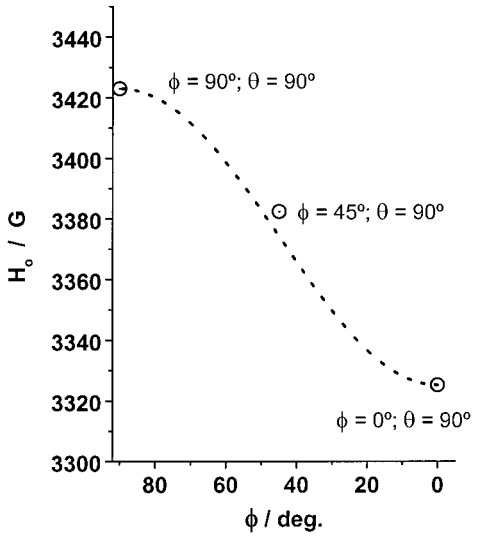

Figure 8. Angular dependence of the resonance field H_o of *cis*-[Mn(2-bzpy)$(N_3)_2]_n$ (**1**) at room temperature and X-band with the orientation of the microwave field for a constant $\theta = 90°$ orientation. $\phi = 0$ and $\phi = 90°$ refer to the orientation of the external field with the chain axis. The dotted line shows the expected dependence of H_o with ϕ according to the cos 2ϕ law.

system, and attributed to short-range interactions. *G*-shifts may also be due to demagnetization effects, but they should become important only at low temperature. In our case, at high temperature these explanations are not acceptable and seem to agree with the angular dependence of *g* pointed out by Benner et al. for TMMC.[24] These authors suggested that, at low symmetry and in the presence of broad lines, transverse dynamic susceptibility $\chi^{xx}(\omega)$ cannot be efficiently described by the circular polarized susceptibility $\chi^{++}(\omega)$, which is generally used in theoretical treatments. They showed that in some cases the nondiagonal contributions, $\chi^{+-}(\omega)$ and $\chi^{-+}(\omega)$, must be taken into account. When this is done, dynamic shifts may be observed in the lines. In fact small shifts were observed in TMMC and $CsNiF_3$.[24]

The proposal of Benner et al. also suggests the dependence of the resonance field (for a constant θ angle), as a function of the microwave field angle ϕ with the chain, following the cos 2ϕ law.[24] In our case this *g*-shift was confirmed by the different resonance fields for $\theta = 90°$ and $\phi = 90$ or $\phi = 0°$ observed during the three rotations of the crystal. In addition, a third spectrum at $\phi = 45°$ was measured. As is shown in Figure 8, compound **1** follows the expected ϕ dependence.

(b) *trans*-[Mn(3-Bzpy)$_2$(N$_3$)$_2$]$_n$ (2). Single-crystal spectra of **2** were recorded by rotating 180° with the static magnetic field in the well-formed (0 0 −1) face. There are two crystallographically equivalent, but magnetically nonequivalent, chains in the unit cell, parallel to the (1 1 0) and (1 −1 0) directions, forming an angle of 68.74° between them, Figure 9. The angular dependence of the line width shows two maxima close to the directions of the chains, and four minima, which nicely agree with the magic angles of the chains. In fact we assume that the spectra in each crystal setting are the sum of two contributions, corresponding to the nonequivalent chains. The two signals have different line widths, and in general the experimental spectrum will have a peak-to-peak width which is close to that of the

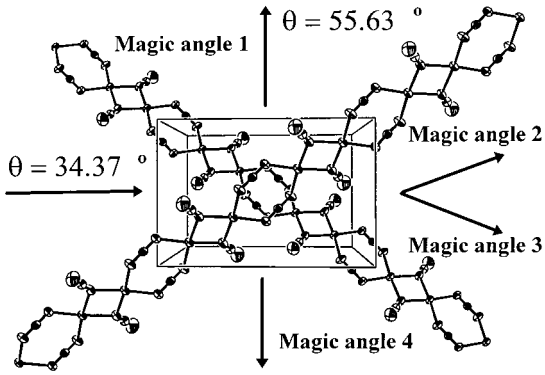

Figure 9. Scheme of the two different chain directions along (1 1 0) and (1 −1 0) for *trans*-[Mn(3-bzpy)$_2$(N$_3$)$_2]_n$ (**2**). Magic angle 1−4 indicate the expected directions at which the magic angle for one set of chains should be found and the two θ common angles for all chains.

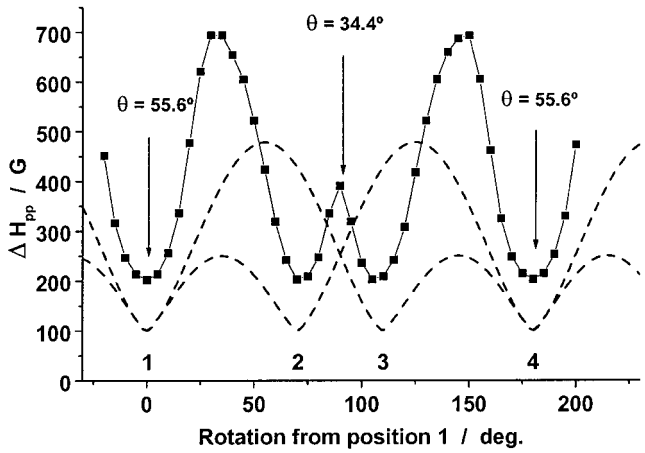

Figure 10. Angular dependence of the peak-to-peak line width ΔH_{pp} of *trans*-[Mn(3-bzpy)$_2$(N$_3$)$_2]_n$ (**2**) at room temperature and X-band. The numbering 1−4 and the two θ angles refer to Figure 9. Dotted lines show the angular dependence $[3\cos^2\theta - 1]^{4/3}$ for the two chains with a θ gap of 68.74°. The solid line is a guide for the eye.

narrower signal. In Figure 10 we show the calculated line widths, assuming a $(3\cos^2\theta - 1)^{4/3}$ behavior. Line shape analysis performed for the equivalent orientations $\theta = 34.37$, 54.7, and 90° shows characteristic one-dimensional behavior, and the expected line widths of 694, 293, and 350 G, respectively. It is also worth noting that **2** also exhibits a *g*-shift as a function of the θ angle, but in this case the effect was less intense than the effect observed for compound **1**. The minimum *g* value of 1.97 was found for $\theta = 34.37°$, and the maximum *g* of 2.03 appears for the perpendicular spectrum; so we tentatively give the same explanation for the *g* shift in **1**.

Therefore, although in this case the analysis of the data is made more difficult by the presence of nonequivalent chains in the lattice which do not permit the $\theta = 0°$ spectrum to be obtained, the EPR data confirm the one-dimensional nature of the interaction.

(c) *cis*-[Mn(3,5lut)$_2$(N$_3$)$_2]_n$ (3). To perform the single-crystal experiments, an indexed crystal of **3** was mounted on the (−1 0 −1) well-developed face. In all the crystal orientations the resonance was observed at $g = 2.00$. As above, three rotations were measured, two of them from parallel to orthogonal to the chain in two orthogonal planes and the third was a rotation with respect to the external magnetic field for a constant $\theta = 90°$ value. The results are apparently surprising: in the first rotation (from 010 to 101), Figure 11, the line width is highest when orthogonal to the chain, and the minimum is at the magic angle

(23) Caneschi, A.; Gatteschi, D.; Zanchini, C.; Rey, P. *J. Chem. Soc., Faraday Trans.* **1987**, *83*, 3603.
(24) Benner, H.; Brodehl, M.; Seitz, H.; Wiese, J. *J. Phys. C* **1983**, *16*, 6011.

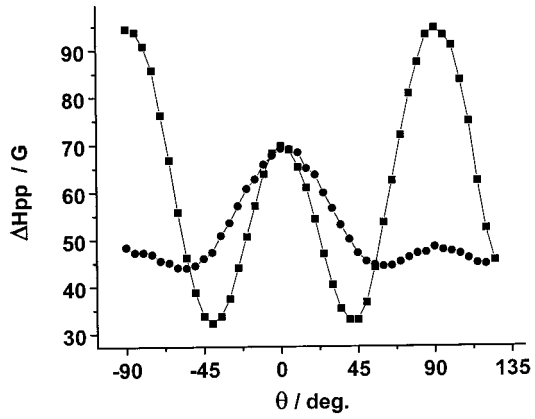

Figure 11. Angular dependence of the peak-to-peak line width ΔH_{pp} of *cis*-[Mn(35lut)$_2$(N$_3$)$_2$]$_n$ (**3**) at room temperature and X-band. The two orthogonal rotations show the normal angular dependence (filled circles) and reversed parallel−perpendicular behavior (solid squares).

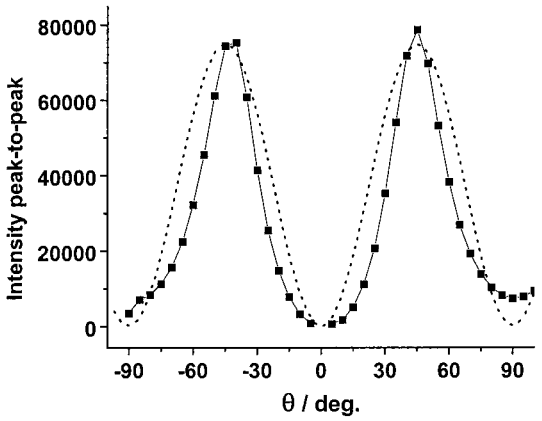

Figure 12. Angular dependence of the intensity of the half-field signal ($g = 4.00$) of *cis*-[Mn(35lut)$_2$(N$_3$)$_2$]$_n$ (**3**) at room temperature and X-band. The signal disappears at $\theta = 0$ and shows maximum intensity for $\theta = 45°$ according to the expected $\sin^2\theta \cos^2\theta$ law (dotted line).

from the perpendicular to the chain. In fact, maximum broadening was found for $\theta = 90°$ (95 G), the magic angle at $\theta = 35°$ (33 G) and the local maximum in the parallel direction $\theta = 0°$ (70 G). In the second rotation (orthogonal to the first rotation), the positions of the maximum and minimum line widths are normal, but the broadening effect is very weak. In the third rotation (constant $\theta = 90°$), a complicated dependence of the line width was observed. The inverse broadening effects for the rotation from 010 to 101 are also reflected in the corresponding line shape analysis, which shows a more diffusive component for the $\theta = 90°$ spectrum and a more Lorentzian component for $\theta = 0°$ and the magic angle.

This surprising feature may be related to the structural data, since the manganese atoms along the chain form a zigzag arrangement with an unusual angle Mn···Mn···Mn of 97°. For this reason the dipolar effects are minimized along the chain axis, and then weak normal or anomalous reversed behavior may be found for selected $\theta = 90°$ orientations.

Due to the narrowing of the main line in the EPR spectrum, a well-defined half-field line is observed at $g = 4.00$. Rotation between $\theta = 0°$ and 90° shows the same line width angular dependence as the main line at $g = 2.00$. According to the expected properties, the intensity of the $g = 4.00$ signal decreases when θ approaches the parallel direction and disappears for $\theta = 0°$. The observation of the half-field line is excellent evidence[19] of the one-dimensional nature of **2**. In Figure 12 the angular dependence of the half-field signal with the expected[25] $\sin^2\theta \cos^2\theta$ law is shown.

Conclusions

Three one-dimensional manganese−azido systems were prepared and structurally characterized. Each compound is characterized by different chain structure and magnetic behavior: double EO bridges by ferromagnetic coupling (**1**), alternating EE and EO bridges by alternating ferro−antiferromagnetic coupling (**2**), and finally EE bridges by antiferromagnetic interactions (**3**). Single-crystal EPR experiments showed that these new types of one-dimensional magnetic materials can be interpreted on the same grounds as were originally developed for the regular Heisenberg antiferromagnet TMMC. Therefore, we have shown that the spin dynamics in one-dimensional ferromagnets and alternating ferro−antiferromagnets can easily be related to the dynamics in antiferromagnets.

Acknowledgment. A.E. and R.V. thank the CICYT (Grant PB96/163) for supporting this research. F.A.M. thanks Prof. C. Kratky and Dr. F. Belaj (University of Graz) for use of experimental equipment. F.A.M. and M.A.M.A.-Y. are grateful for partial support from an OENB grant (Project 6630). D.G. thanks the EU for the TMR Grant 3MD.b.

Supporting Information Available: Three X-ray cryatallographic files, in CIF format. This material is available free of charge via the Internet at http://pubs.acs.org.

IC990656X

(25) Benner, H.; Wiese, J. *Physica B* **1979**, *96*, 216.